Finding the right substrate support for magnetic superatom assembly from density functional calculations

Akansha Singh and Prasenjit Sen*
Harish-Chandra Research Institute, Chhatnag Road, Jhunsi, Allahabad 211019, India
(Received 17 September 2014; published 28 January 2015)

In order to find the right support to form assemblies of superatoms with useful magnetic properties, adsorption of the magnetic superatom $FeCa_8$ on different types of substrates is studied using first-principles electronic structure methods. $FeCa_8$ interacts strongly with oxide and metal substrates and its structure and magnetic properties are destroyed. Interaction between $FeCa_8$, and graphene and hexagonal BN (h-BN) are weak, and its structure is retained on these substrates. Dimers of $FeCa_8$ are also found to be stable on both h-BN and graphene. While the magnetic interaction between two $FeCa_8$ units deposited on h-BN involves only direct exchange, substrate mediated RKKY interaction also plays a role on graphene. Consequences of these for the magnetic properties of the assemblies are discussed.

DOI: 10.1103/PhysRevB.91.035438 PACS number(s): 31.15.A−, 68.43.−h, 36.40.Mr, 61.46.Bc

I. INTRODUCTION

One of the most exciting outcomes of years of research on small metal clusters [1,2] has been superatoms [3–10]. The idea was first proposed in the mid 1990's based on the observation that electronic structure of some simple metal (alkali [11,12], alkaline earth [13,14], coinage metal [7]) clusters obey the so-called shell models [2,15]. Since atoms tend to attain filled shell electronic configurations in order to gain stability, it was argued that metal clusters mimic this behavior and hence could mimic properties of elemental atoms on the periodic table [3]. Since then the existence of superatoms has been established firmly through experimental demonstrations and first-principles electronic structure calculations [4,9]. In a recent review article, Castleman and Khanna [16] have given the currently accepted definition of a superatom. Atomic clusters that retain their identity in assemblies and posses properties like analog atoms have been termed superatoms. Castleman, Khanna, and co-workers [4–6] have demonstrated that many atomic clusters, notably Al_{13}, Al_{13}^-, Al_{14}, and Al_7^-, behave as superatoms. Out of these, Al_{13} behaves as a halogen atom and has been termed a superhalogen, Al_{13}^- behaves like an inert gas atom, Al_{14} mimics properties of alkaline earth atoms while Al_7^- behaves as a multiple valence superatom. Possibility of an ionic bonded molecule formed by K and Al_{13} was also established through first-principles calculations [17]. This has recently been established experimentally [18]. In addition, theoretical works by Khanna *et al.* [19] showed that the A_3O species acts as superalkali (A=alkali atoms).

While these were exciting developments, all these superatoms were nonmagnetic. Having the origin of their stability in filled electronic shells, there was no way for these superatoms to posses magnetic moment. A breakthrough in the direction of producing magnetic superatoms came in 2009 when one of us along with Khanna *et al.* [11] showed that VCs_8 and ligated $MnAu_{24}$ act as magnetic superatoms. Since then, many other magnetic superatoms have been identified. One of the qualifying criteria used to decide whether a stable magnetic cluster is a superatom or not is to try and form dimers of it. This is the first test whether it would be stable in assemblies and whether it would retain (at least part of) its magnetic moment. For example, although both VNa_8 and VCs_8 turn out to be stable clusters within the respective VA_n series (A=Na, Cs), two VNa_8 clusters, when put together, merged completely to form a V_2 dimer surrounded by sixteen Na atoms, and lost their magnetic moments. Therefore, by the modern definition, VNa_8 does not qualify as a magnetic superatom. VCs_8, on the other hand, retained its identity and formed stable dimers and trimers with distinct magnetic properties. Similarly, dimers of $FeMg_8$ [9], $FeCa_8$ [13], $CrSr_9$, and $MnSr_{10}$ [13] were found to be stable in which individual cluster units retain their identity. Therefore these stable clusters qualify as magnetic superatoms.

As we have already stated, it is important for the stable cluster unit to retain its structural identity and magnetic properties in assembly for it to qualify as a magnetic superatom. In all the theoretical works involving magnetic superatoms mentioned above, the assemblies have been studied in the gas phase, i.e., their free-standing dimers [11] and trimers have been studied. However, for these superatoms to be useful in building cluster assembled materials, such assemblies have to be made in a form that can be made to rest. For example, assemblies can be made either in zeolite cages or on substrate supports. In fact, cluster assemblies obtained by depositing preformed size selected (or otherwise) clusters on a chosen substrate through low-energy cluster beam deposition (LECBD) technique is a well studied subject [20–28]. Deposition and self-assembly of magnetic superatoms will lead to production of magnetic thin films whose properties can be tuned by choosing the building blocks, i.e., the superatoms. These may open new avenues in spintronic and magnetic storage materials. In fact, Khanna *et al.* have shown that a dimer of two VCs_8 units acts as an efficient spin polarizer [29]. It would be interesting to extend such ideas to larger assemblies of these superatoms.

In order to form useful assemblies of magnetic superatoms, proper substrates have to be identified. Some of the desirable properties of a substrate are that (1) the superatom-substrate interaction has to be weak enough so that the superatom retains it structural identity. If the superatom-substrate interaction is much stronger than the intracluster interactions, it would tend to wet the surface thereby losing its structural identity. This is likely to destroy its magnetic property also. (2) Even if the

*Corresponding author: prasen@hri.res.in

superatom retains its structural identity, it is not guaranteed that its magnetic moment will be retained. The superatom-substrate interaction should be such that a substantial part of the magnetic moment of the free superatom is maintained even after deposition. (3) When two or more superatoms are deposited on the substrate they should have an interaction strength so that they each retain their structural identity. Ideally, they should retain their magnetic moments also. However, it is possible that they may not retain the entire moment of an isolated superatom while forming the assembly. This is true of elemental atoms also. For example, an isolated Fe atom has a moment of 4 μ_B because of its $3d^6 4s^2$ configuration. An Fe_2 dimer [30], in its lowest-energy state, has a moment of 6 μ_B rather than 8 μ_B, and bulk ferromagnetic Fe has 2.2 μ_B per atom [31].

Clearly, this is a stringent set of requirements for a substrate to be useful for assembly of a particular magnetic superatom. It is possible that different substrates may be ideal for different superatoms. To explore these issues, we take $FeCa_8$ as a prototypical example and explore its properties on different types of substrates commonly used. Chauhan etal have shown that $FeCa_8$ behaves as a magnetic superatom [13]. Here we study alumina ($\alpha - Al_2O_3$), fcc calcium, graphene, and hexagonal BN (h-BN) as possible substrates. Alumina has been chosen as a representative oxide substrate. Oxide substrates such as Al_2O_3, TiO_2, CeO, and MgO are routinely used to deposit clusters for various applications, most notably catalysis. Calcium surface is chosen as an example where the cluster-surface interaction is expected to be of the same strength as the intracluster interaction since most of the clusters atoms are also Ca. Graphene and h-BN are chosen because these are two-dimensional materials with no dangling bonds at the surface [32], and hence are expected to interact weakly with the superatom. Compared to Al_2O_3, the degree of ionicity is also expected to be small in h-BN. Indeed, studies [33–38] have shown that interactions between these (as also graphite) and metal atoms are dominated by dispersion forces, and are very weak. Metal adatoms are trapped only at defect sites and step edges on a graphite substrate. Recently, an experiment [38] has also confirmed the presence of van der Waals interaction between a topological insulator and h-BN substrate.

We try to identify the substrate(s) on which an individual $FeCa_8$ cluster retains its structural identity and magnetic moment. We then try to form assemblies of two $FeCa_8$ units on such substrates. Our calculations show that graphene and h-BN are promising supports for magnetic superatom assemblies.

In Sec. II, we present the theoretical approach used for these calculations. In various parts of Sec. III, we present results for structure and energetics and electronic structure of $FeCa_8$ deposited on the four substrates mentioned above. We also present results of two $FeCa_8$ units deposited on h-BN in Sec. III C. Finally, we draw our conclusions in Sec. IV.

II. METHOD

All our calculations are performed within the framework of the density functional theory (DFT). The wave functions are expressed in a plane-wave basis set with an energy cutoff of 400 eV. Interaction between the valence electrons and the ion cores is represented by the projector augmented wave (PAW) potentials [39,40]. $Al_2O_3(0001)$ surface is modeled by a 4×4 supercell with nine atomic layers in a slab in a repeated slab geometry. Top five atomic layers are allowed to relax, while the bottom four layers are held fixed in their bulk terminated positions. This choice of in-plane supercell size ensures that the nearest distance between cluster atoms in the simulation cell and their periodic images is $\sim$ 13Å. We believe this is enough to ensure absence of any direct electronic interaction between them. Dipole corrections were included to avoid any spurious interaction between periodic images of the slab due to long-range dipole-dipole interactions [41]. The (001) surface of fcc calcium is represented by a 5×5 supercell with seven layers in the slab. This also ensures that the minimum distance between cluster atoms and their periodic images is more than 13 Å. All the atoms are allowed to relax during structure optimization. For both these surfaces, a vacuum of 15 Å is included between a slab and its periodic image. h-BN-sheet is represented by a 7×7 supercell in the plane for deposition of a single $FeCa_8$ unit, and by 11×11 and 14×14 supercells while depositing two $FeCa_8$ units. For graphene, we used supercells of various sizes increasing from (4×4) to (13×13) (lateral dimensions of 9.9 to 32.2 Å). A vacuum space of 20 Å separating two successive sheets has been used for both h-BN and graphene. The Brillouin zone (BZ) integrations were performed using the Γ point only in all cases except for graphene when studied using (4×4) and (5×5) unit cell. For these two sizes, we used 5×5 and 3×3 **k**-point grid, respectively. The Vienna *ab initio* simulation package (VASP) [42] was used for all our calculations.

Different functionals were used to represent the exchange-correlation energy in different situations. For $FeCa_8$ supported over alumina and calcium surfaces, we used the local spin density approximation (LSDA). For metal atoms on graphene and h-BN substrates, dispersion forces play important roles and the treatment of these dispersive forces have always been a challenge for first-principles theories. Standard local and semilocal functionals within DFT are not capable of describing such interactions. Two different approaches are usually taken to incorporate these interactions: a semiempirical approach suggested by Grimme [43–45], and using a nonlocal correlation functional [46–50]. Recent works by us [51] and other researchers [33] have shown that the semiempirical approach leads to incorrect binding sites for Ag atoms on graphene/graphite. We have also shown that the behavior of Ag clusters on a graphite substrate can be described correctly only by using the nonlocal functionals. Therefore we have used the vdW-DF2 [52–54] method which incorporates dispersion interaction through a nonlocal correlation functional. Within this approach, the exchange-correlation energy E_{xc} is split up as $E_{xc} = E_x^{GGA} + E_c^{LDA} + E_c^{nl}$, where E_x^{GGA} is the exchange-energy in the revPBE approximation [55], E_c^{LDA} is the local correlation energy calculated within LDA, and the nonlocal correlation energy E_c^{nl} is calculated by the kernel developed by Dion *et al.* [49].

Before the development of the nonlocal correlation functionals, a number of studies on metal-graphite or metal-graphene systems used the LSDA within DFT. For a comparison with our vdW-DF2 calculations, and to establish the fact that one may get qualitatively different results in these two

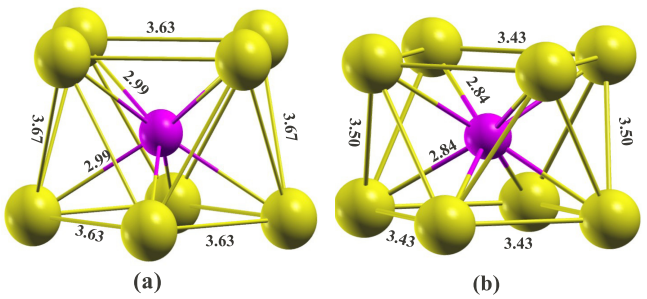

FIG. 1. (Color online) The lowest-energy structure of $FeCa_8$ using (a) vdW-DF2 and (b) LSDA.

methods, we present our LSDA results on these two systems in Appendix.

III. RESULTS AND DISCUSSIONS

Before depositing a $FeCa_8$ superatom on substrates, one has to find its ground-state structure and electronic structure. These, of course, were studied thoroughly in Ref. [13]. However, those calculations were performed using an atom-centered Gaussian basis set [56]. Here we use plane wave basis set. Therefore we need to recalculate the isolated cluster using this method. For calculation of an isolated cluster, it was placed at the center of a periodic cubic box of dimensions 25 Å in each direction. Energy cutoff for the plane-wave basis and other details of the calculations were as described in Sec. II.

A. Isolated $FeCa_8$ superatom

Figure 1 shows the optimized structures of the $FeCa_8$ cluster obtained using the LSDA and vdW-DF2 methods. $FeCa_8$ has a square antiprism structure with an endohedral Fe atom, as found earlier using PBE [57]. In order to explain its electronic structure, we have plotted the energies of the Kohn-Sham orbitals, and the partial charge densities coming from these in Fig. 2. $FeCa_8$ is found to have a $1S^2 1P^6 1D^{10} 2S^{22} D^4_\alpha$ electronic configuration in both vdW-DF2 and LSDA in agreement with Ref. [13]. S, P, D refer to the angular momentum character of the cluster molecular orbitals (MO) in conformity with the spherical shell models. α is used to denote the majority spin channel. A detailed discussion about the origin of stability of this cluster can be found in Ref. [13]. Although they give the same electronic configuration, there are subtle differences between the vdW-DF2 and the LSDA results in orderings of different molecular orbitals, and their splittings. For example, in LSDA, 1D states of the cluster split in groups of 2 and 3 degenerate states in the α channel. In vdW-DF2 as in PBE [13] this spilling is 4 and 1. In vdW-DF2, the 1S orbital is followed by the four degenerate 1D orbitals in the α-spin channel, and in LSDA it is followed by two degenerate 1P orbitals. In both cases, the Ca-Ca distance within the square planes of the antiprism is larger than the vertical distance between the two square planes. Thus these structures can be viewed to have oblate distortions relative to a more symmetric "spherical" structure in the language of electronic shell models, an idea that has been elaborated in detail in previous works on these superatoms. The ratio of the vertical distance between the planes and the in-plane Ca-Ca distance turned out to be 0.85 and 0.91 in vdw-DF2 and LSDA, respectively. Ratios between the vertical distance and the in-plane diagonals and the body diagonals in the two cases are also slightly different. This difference in the amount of "distortion" may be responsible for the slightly different electronic structures.

B. $FeCa_8$ adsorbed on substrates

Having found the ground state of the $FeCa_8$ cluster, we now try to find its structures and properties on the substrates. In LECBD experiments, clusters can land on the substrate

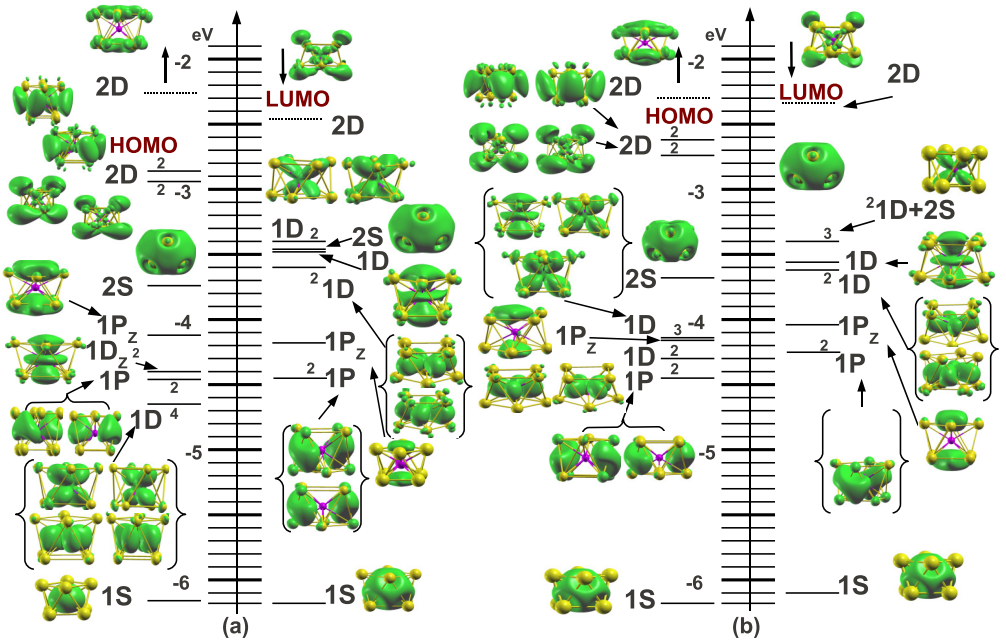

FIG. 2. (Color online) The MO's, and corresponding charge densities of $FeCa_8$ using (a) vdW-DF2 and (b) LSDA. Degeneracy of the MO's are also indicated.

randomly at all possible positions and in all possible orientations. To mimic this process, we generate initial structures of the deposited clusters in the following way. A $FeCa_8$ cluster is placed above the substrate so that its center of mass is at some height above the special symmetry points of the surface. For the Al_2O_3 surface, four adsorption sites Al1, O2, Al3, and O5 [shown in Fig. 11(a) in Appendix] are considered. For calcium surface, we choose on-top Ca-site (T) and fourfold hollow site (H). For the graphene and h-BN substrates, the top site(s) (B and N atoms in case of BN), the bridge site and the hollow site are chosen. At each of these sites it is ensured that the closest distance between the substrate and cluster atoms remains greater than the sum of their atomic radii. While generating the initial structures, the clusters are treated as rigid bodies. Their random orientations are generated by choosing the Euler angles randomly. A number of different orientations of the cluster are generated at each site. All these initial structures are then relaxed to their nearest local minima. Sometimes different initial structures relax to the same final geometry after relaxation.

Relative stability of different final structures on a particular substrate is measured by comparing the adsorption energies. Adsorption energy of the cluster in a particular structure is defined as

$$E_a = E_T(\text{substrate}) + E_T(\text{FeCa}_8) - E_T(\text{FeCa}_8/\text{substrate}). \quad (1)$$

E_T's are the total energies of the respective systems.

1. Alumina substrate

Before depositing $FeCa_8$ on the alumina substrate, we calculated properties of bulk alumina. Using the local density approximation, we obtained lattice parameters $a = 4.61$Å and $c = 13.6$Å, which are in good agreement with the experimental values [58]. Bulk α-alumina is an insulator with a direct gap of 8.8 eV [59]. Our calculated band gap is 6.68 eV, exhibiting the usual underestimation of band gaps in the LDA. We took several initial structures for $FeCa_8$ on the $Al_2O_3(0001)$ surface and relaxed these to their nearest local minima. Figure 3(a) shows the lowest-energy structure obtained in this way.

It is clear that the antiprism motif of the cluster is completely destroyed and the endohedral Fe atom is exposed to the alumina surface. Such a large deformation of the $FeCa_8$ unit is a consequence of a very strong interaction between the cluster and the substrate. This is proven by the fact that the adsorption energy of $FeCa_8$ on Al_2O_3 in this lowest-energy structure is 13.46 eV. This is much larger than, for example, the adsorption energy of Ag_8 on graphite [51], which is 0.71 eV. As we will see later, interactions between $FeCa_8$ and graphene and h-BN are also rather weak. The requirement for a substrate to be a good support for superatom assembly, that the cluster-substrate interaction be weak, is clearly not met by Al_2O_3. As a consequence, the electronic structure and magnetic properties of $FeCa_8$ also change substantially. Most importantly, the magnetic moment of the isolated superatom is lost after adsorption. The immediate reason for this is a large charge transfer to the substrate. We calculated the Bader [60] charges on all the atoms in the final relaxed structure, and find that a charge of $4.8e$ (e is electronic charge) is transferred from the cluster to the substrate. Most of the charge is transferred from the Ca atoms of the cluster to the neighboring Al atoms of the substrate. The density of states plot for this system is shown in Fig. 12. It turns out that all the energy states of the gas phase cluster lie within the band-gap region of the alumina slab. After deposition, also a set of discrete states are found in the gap region, which are localized on the cluster atoms and the nearby Al atoms. An equal number of such states appear in the two spin channels, and hence there is no magnetic moment.

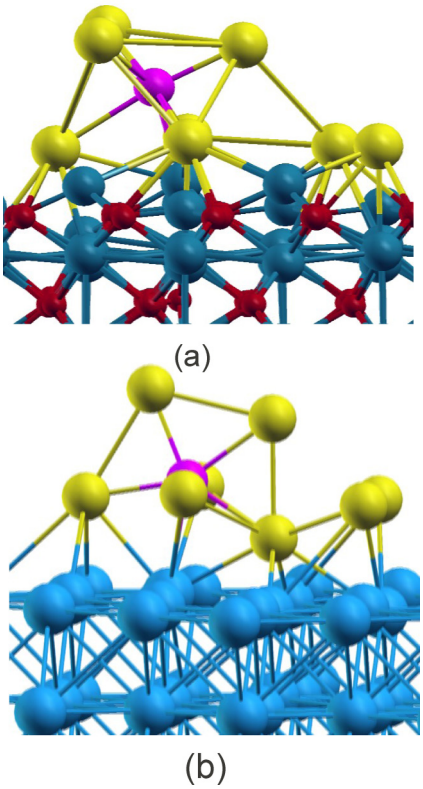

FIG. 3. (Color online) The lowest-energy structure of $FeCa_8$ supported over alumina (a) and calcium (b) substrates. In (b), the substrate Ca atoms are shown with a darker (blue) color to distinguish them from the Ca atoms of the superatom.

2. Ca substrate

Next, we explored the adsorption of the $FeCa_8$ cluster on the Ca(100) surface. First, we calculated properties of the bulk fcc calcium. Our calculated cubic lattice parameter is 5.32 Å within LDA. This compares well with the experimental value of 5.582 ± 4Å [61]. We took several initial structures for $FeCa_8$ over Ca(100) and relaxed them to their nearest local minima. In the lowest-energy structure [Fig. 3(b)], the cage of the cluster is deformed and the Fe atom is exposed to the surface as on the alumina substrate. Strong interaction between the cluster and the substrate leads to a fairly large adsorption energy of 5.75 eV. Due to this strong interaction, the electronic states of the cluster are also heavily modified and the magnetic moment of the cluster is completely lost. The density of states for $FeCa_8$ on Ca(100) is shown in Fig. 13. Metallic Ca has finite DOS around the Fermi energy. The cluster states are heavily mixed with the Ca states. States around -1.25 eV, and from the Fermi energy up to $\sim$1.9 eV have significant contributions both from

the substrate and the cluster. We also found a charge transfer of 0.94e from cluster to the surface.

3. *Graphene and h-BN substrates*

Having found out that alumina and Ca substrates are not appropriate supports that preserve properties of the $FeCa_8$ superatom, we now explore graphene and h-BN sheets as possible supports. For reasons discussed earlier, we have used the vdW-DF2 method, while studying $FeCa_8$ on these substrates. Only for the sake of comparison, we briefly present our LSDA results in Appendix.

h-BN is an insulating material with a nearest-neighbor bond length 1.45 Å and a measured band gap of 5.97 eV [62]. Within the vdW-DF2 method, the optimized nearest-neighbor B-N distance turns out to be 1.454 Å, and the calculated band gap is 4.52 eV.

We took several initial structures for $FeCa_8$ on the h-BN sheet and relaxed these to their nearest local minima. In complete contrast to alumina and calcium substrates, the $FeCa_8$ cluster retains its square antiprism motif in all the structures. This is the first encouraging sign that h-BN may be a good substrate for superatom assembly. In the lowest-energy structure [Figs. 4(a) and 4(b)], one of the square planes of the antiprism structure is aligned parallel to the h-BN sheet. Three of the Ca atoms are at on-top sites, while the fourth one is near a hollow site. There is very little change in the bond lengths in the cluster. The Ca-Ca bond lengths in the square plane close to the substrate increase marginally by 0.02 Å. The other bond lengths remain as in the isolated cluster. $FeCa_8$ has an adsorption energy of 0.82 eV in this structure.

Another structure having one Ca atom at a top site, two at hollow sites and the fourth one at a bridge site is only 6 meV higher in energy. Structures with smaller number of Ca-B/N neighbors are found to be higher in energy. To illustrate the point further, we show two other structures in Fig. 14 in the Appendix. In the structure in Fig. 14(a), only two Ca atoms are close to the surface. This structure is 21 meV higher than the lowest-energy structure. The structure in Fig. 14(b), having only one Ca atom close to the surface, is 0.27 eV higher than the lowest-energy structure.

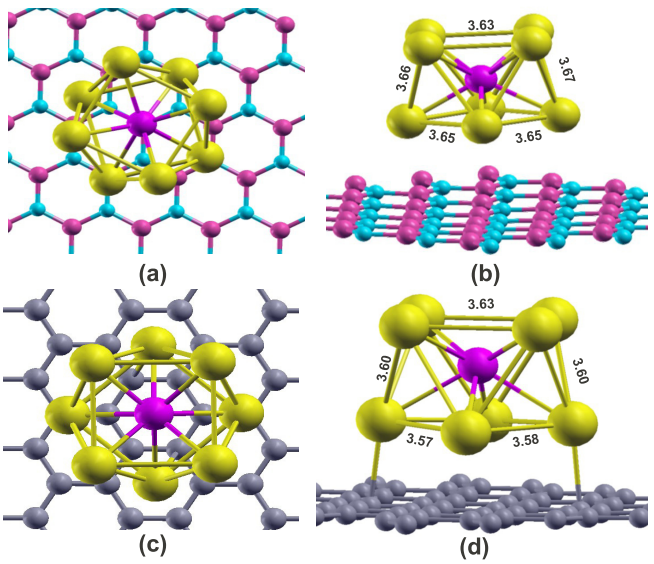

FIG. 4. (Color online) The lowest-energy structure of $FeCa_8$ supported over h-BN sheet (a) and Graphene (b) using vdW-DF2. First column: top view; second column: side view.

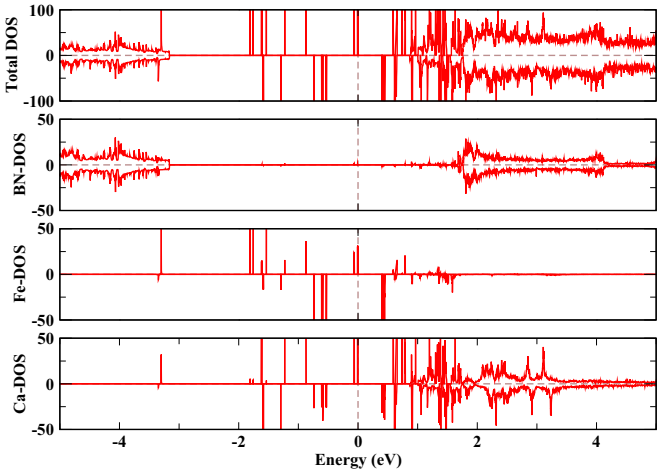

FIG. 5. (Color online) Total density of states, and atom projected partial density of states of h-BN supported $FeCa_8$.

In the lowest-energy structure, the minimum distance between the surface and cluster atoms is 3.87 Å. This large cluster to surface distance rules out any chemical bond between them and suggests a physisorption scenario. While the superatom retains its antiprism motif after deposition, we also measure the deformation of the surface by calculating two quantities: relaxation of the surface atoms from their initial positions (Z_r) and the deviation of the individual surface atoms (Δz_s) from their average z coordinates (perpendicular to the surface). For the lowest-energy structure, maximum z_r is 0.28 Å, while the maximum Δz_s is 0.24 Å. These are found for the B atom directly below the Fe atom of the cluster.

Now we look at the magnetic and electronic properties of the $FeCa_8$ on h-BN. In the lowest-energy adsorbed structure, the magnetic moment turns out to be 4 μ_B. Thus the magnetic moment of the isolated $FeCa_8$ cluster is retained entirely after deposition. To understand the electronic structure of the combined cluster-substrate system, we analyze its density of states (DOS) as shown in Fig. 5. Most of the occupied cluster states lie within the band gap region of the BN sheet and have little mixing with the surface states. This is in clear contrast to the $FaCa_8$/alumina system in which the localized states had contributions both from the cluster and the surface atoms close to it. This lack of mixing preserves the MO's on the cluster nearly exactly, which we have also confirmed from the partial charge density. In particular, the four 2D states in the majority spin channel responsible for the magnetic moment in the isolated cluster appear right at the Fermi energy in the supported cluster. This preserves the moment of 4 μ_B. Indeed, most of the moment is localized on the cluster as seen in the spin density isosurface plot shown in Fig. 15. From this it is clear that a h-BN sheet is an ideal support for a magnetic superatom such that its structural and magnetic properties remain unaffected.

Some of the higher energy structures also preserve the magnetic moment of the isolated cluster. For example, the structure shown in Fig. 14(a) has a magnetic moment of 4 μ_B. Its structural motif is very similar to the gas phase cluster, which preserves the MO's of the cluster. The structure in Fig. 14(b) on the other hand, which has only one Ca atom close to the substrate, loses part of its moment after deposition, and has a moment of 2 μ_B. This is because there is substantial distortion of the superatom geometry in this structure. As has been discussed by Chauhan *et al.* [13], the particular antiprism structure with an oblate distortion is crucial in obtaining a moment of 4 μ_B. To illustrate this point further, we show a scatter plot of E_a vs magnetic moment of $FaCa_8$ on h-BN in Fig. 16. In addition to the three structures discussed so far (Figs. 4 and 14), an additional structure is also shown in which the superatom completely loses its moment. The superatom undergoes the maximum distortion in this structure leading to the complete loss of moment.

Next, we study adsorption of $FeCa_8$ on a graphene substrate. Our calculated C-C bond length in a graphene sheet turned out to be 1.43 Å within vdW-DF2, marginally larger than the experimental value (1.42 Å) but in agreement with previous theoretical results [48]. We also found two Dirac cones in the electronic structure at the K and K' points of the BZ, as expected.

Graphene is an interesting substrate because it has been shown that magnetic moments on a graphene sheet are coupled through RKKY interactions mediated by the π electrons [63–65]. However, unlike a usual two-dimensional metal, the RKKY interaction on graphene has a $1/R^3$ asymptotic behavior [63] due to its suppressed DOS at the Fermi energy. It has also been shown that the interaction is oscillatory but always anti-ferromagnetic for moments located on two different sublattices [64]. For moments located on the same sublattice, the oscillatory interaction remains ferromagnetic at all distances. If the moments are located at the hollow sites [64], the interaction is antiferromagnetic, and goes down monotonically with distance as $1/R^3$. It has also been argued that the RKKY interaction on graphene can be very long ranged, extending up to 50 Å [66]. This poses an immediate challenge for first-principles calculations. In order to study adsorption of an isolated superatom, the graphene sheet has to be ~ 50 Å in each direction. This is computationally very expensive. Therefore we study adsorption of a $FeCa_8$ cluster on graphene sheets of increasing lateral extent. It is understood from the above observations that there will be magnetic exchange interaction between the $FeCa_8$ cluster in the simulation supercell and its periodic images in the lateral directions. Our goal is to extract an estimate of the distance dependence of the exchange interaction, and not necessarily to study properties of an isolated $FeCa_8$ on graphene. Usually, such estimates are made from a difference in the energies of the ferromagnetic and antiferromagnetic alignments of two fixed moments [64,66]. However, with a single unit of $FeCa_8$ in the supercell that is not possible. Having two units of $FeCa_8$ is also not meaningful because of the long-range nature of the interaction (more on it later).

We calculated energies of a $FeCa_8$ cluster on a graphene sheet both in the nonmagnetic state, and with the moment fixed to that of the isolated superatom, i.e., 4 μ_B. A difference

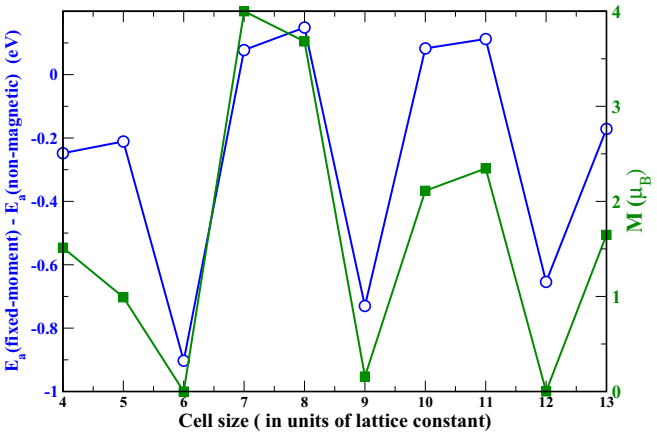

FIG. 6. (Color online) Difference in the adsorption energies (circle) of $FeCa_8$ having magnetic moment of 4 μ_B (fixed-moment) and no magnetic moment (nonmagnetic) on a graphene sheet represented by supercells of various sizes; and the moment (square) obtained through self-consistent calculations (M).

in the two energies gives an estimate of the magnitude of the magnetic interaction. Lehtinen *et al.* [67] adopted a similar strategy to establish the existence of RKKY interactions between magnetic moments on adatoms on graphene.

Before this we took various random orientations of $FeCa_8$ over a (7×7) graphene sheet and relaxed them to their nearest local minima. Just as on h-BN, the $FeCa_8$ cluster retained its square antiprism motif in all the structures. The lowest energy is obtained for a structure in which four Ca atoms stay close to the graphene sheet [Figs. 4(c) and 4(d)], two being above hollow sites, and two above top sites. In the lowest-energy structure, the minimum distance between the Ca and the C atoms is 2.66 Å, just about equal to the sum of their atomic radii, indicating a weak cluster-substrate interaction. The maximum Z_r and ΔZ_s are found to be 0.10 and 0.12 Å, respectively. It is quite intriguing that in spite of a closer cluster-substrate distance on graphene, $FeCa_8$ causes a larger deformation in h-BN sheet. We believe this has to do with the stiffness of the flexural phonon modes in these two materials. At large wave vectors, the flexural phonon modes in h-BN are much softer compared to those in graphene [68]. This leads to an easier deformation of a h-BN sheet.

We plot the difference between the adsorption energies of $FeCa_8$ in the nonmagnetic state and with a fixed moment of 4 μ_B with varying cell size in Fig. 6. The cell size is presented in units of lattice constant ($a_0 = 2.476$ Å) and is the same along the two perpendicular in-plane directions. In addition, we also show the moments obtained through self-consistent calculations to produce the lowest energy. It is clear that the energy difference, and hence the exchange interaction strength, has an oscillatory behavior with distance. It is worth noting that while the strength of the exchange interaction (direct plus RKKY) is $\sim 10^2$ meV as seen in Fig. 6. We made an estimate of the magnetic dipole-dipole interaction between the moments on two superatoms at a distance of ~ 9.9Å apart (the distance between a superatom and its periodic image on a 4×4 supercell). This is found to be $\sim 10^{-4}$ meV, six orders of magnitude smaller. Dipole-dipole interaction goes

down monotonically as $1/R^3$. Therefore its contribution to intersuperatom interactions at still greater separations will be insignificant.

At cell sizes of 6, 9, and 12, the nonmagnetic state is favored over the magnetic state by large energies. And indeed at these sizes the self-consistent moments turn out to be nearly zero. At cell sizes 7, 8, 10, and 11, the energy difference indicates the magnetic state to be more favorable. The self-consistent magnetic moment in fact has high values at these sizes. Thus we establish a graphene mediated distance dependent oscillatory exchange interaction between $FeCa_8$ superatoms. To establish that this interaction is not present on a h-BN substrate, we calculated adsorption of $FeCa_8$ on h-BN sheets of increasing size (beyond 7×7). No size dependence of adsorption energy or magnetic moment was found in this large-gap insulating material.

Thus individual $FeCa_8$ superatoms retain their structures both on h-BN and graphene. On h-BN they also retain their magnetic moments in the low-energy structures. Magnetic moment of graphene supported $FeCa_8$ is more complicated because of long-range RKKY interactions.

C. Two $FeCa_8$ units on h-BN

Having established that h-BN is an ideal support with weak enough cluster-support interaction to preserve the structure and magnetic properties of a $FeCa_8$ unit, we now address the question whether two units of $FeCa_8$ form a stable dimer on it and what magnetic states this may have. When a large number of clusters land on the substrate in LECBD experiments, their relative orientations will also be random. The magnetic interaction between two cluster units will in general depend on their relative location and orientation. It is virtually impossible to do a thorough study of all such structures on the substrate within a first-principles approach. Instead, we take a simplified view, which will be relevant when the cluster flux and coverage are low. We consider a situation in which two cluster units have already landed on the substrate in their lowest-energy structures, and then approach each other. While this greatly reduces the number of possible structures one has to consider, the clusters can still approach each other along arbitrary directions on the plane of the substrate. It will still be computationally prohibitive to consider all such possibilities. To make things even simpler, we consider two situations: (1) when two triangular faces of two clusters are connected directly, i.e., each atom of one triangular face is connected to only one atom of the other triangular face [Fig. 17(a)], and (2) when one of the triangular faces is twisted relative to the other and one atom of each triangular face is connected to two atoms of the other face [Fig. 17(b)]. These results should, therefore, be taken in the spirit that they give an indication of whether stable assemblies of $FeCa_8$ clusters are possible on h-BN rather than a quantitative information about possible low-energy structures of such assemblies.

First, we deposit the $FeCa_8$ clusters close to each other in both orientations (discussed above) so that the nearest Ca-Ca distance between them is 3 Å. Figure 7 shows the relaxed structure of such a dimer. In both the orientations, the $FeCa_8$ units retain their individual identities. This structure in Fig. 7 has an adsorption energy of 3.72 eV. Adsorption energy of a single unit in h-BN is 0.82 eV as mentioned earlier. Thus the binding energy between the two units of $FeCa_8$ is 2.03 eV, which is slightly smaller than the binding energy of two units of $FeCa_8$ in gas phase, which is 2.12 eV. Incidentally, this structure is not the lowest-energy structure for the dimer in gas phase. In this structure, the dimer turns out to have a magnetic moment of 2 μ_B. Although this is much smaller than the possible maximum of 8 μ_B for parallel alignment of spins on the two cluster units, the same structure in the gas phase also has a moment of 2 μ_B. Thus there is no additional reduction in moment due to the substrate. Therefore h-BN turns out to be an ideal support that preserves magnetic moments of individual superatoms and their assemblies. Our attempts to study anti-parallel alignment of moments on the two superatom units in this structure were not successful as at the end of the self-consistent calculations, the dimer converged to the same spin state as above with a moment of 2 μ_B.

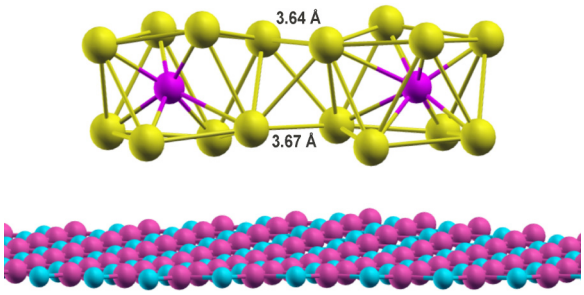

FIG. 7. (Color online) Dimer of $FeCa_8$ deposited over h-BN sheet using vdW-DF2.

We then wanted to understand two other aspects of assemblies of $FaCa_8$ superatoms on h-BN: (i) the distance dependence of interaction between two $FeCa_8$ clusters deposited on h-BN: at what distance do they interact with each other? (ii) What is the strength of long-range dipolar interaction between two superatom units? When we put two units far apart so that the nearest Ca-Ca distance between them is 8.5 Å, the clusters stay in their respective positions. For this calculation we use a 14×14 supercell of h-BN. The total moment turns out to be 8 μ_B, sum of the moments on individual clusters. The adsorption energy is found to be 1.93 eV, only slightly larger than the sum of adsorption energies of the individual clusters. All these show that the two clusters do not feel each other's presence at this distance. On the other hand, when two clusters are placed such that the nearest Ca-Ca distance between them is 5 Å, they approach each other and finally form a dimer as in Fig. 7 with the same magnetic moment of 2 μ_B. These results are further proof of the fact the only magnetic interaction between two $FeCa_8$ units on h-BN is direct exchange. Average intercluster distances of 5 and 8.5 Å correspond to surface densities of 12.73×10^{13} and 4.97×10^{13} per cm^2 respectively. Therefore our results suggest that up to an areal density of 4.97×10^{13} per cm^2, the clusters behave as isolated units on a h-BN substrate, but somewhere between 4.97×10^{13} per cm^2 and 12.73×10^{13} per cm^2, they self-assemble to form new structures. Strength of dipolar interactions are estimated by calculating the energy difference between the ferromagnetic and antiferromagnetic orientations of the spin moments. As stated earlier, we could not stabilize

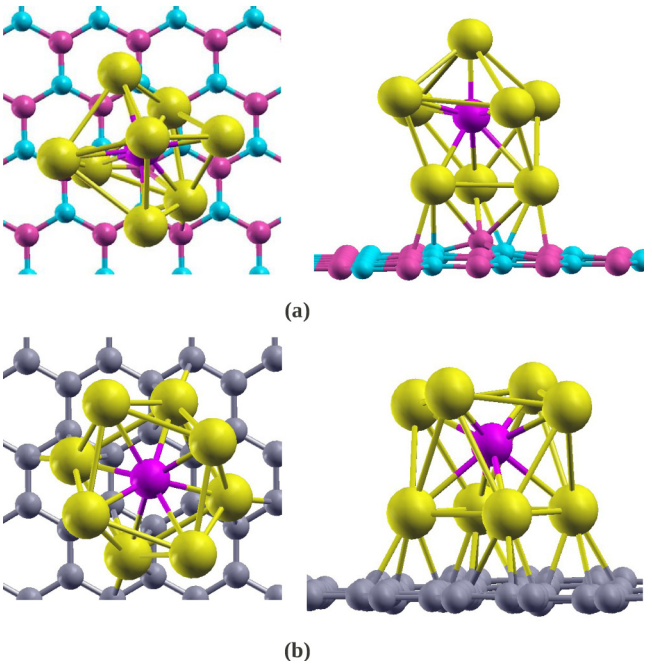

FIG. 8. (Color online) Lowest-energy structure of $FeCa_8$ supported over h-BN sheet (a) and graphene (b) using LSDA method. First column-top view; second column-side view.

the antiferromagnetic alignment of the two superatom spins when they are close to each other. At 5 Å apart, also, their interaction is dominated by electronic exchange, as shown. At a distance of 8.5 Å apart, we could estimate the value of the dipolar interaction strength. It turned out to be only ∼3 meV with the AFM arrangement being marginally lower in energy.

We attempted to study two $FeCa_8$ units on a graphene sheet. In this case, two superatom units in the simulation cell have a direct exchange, and also have RRKY interaction with each other, and their periodic images. All these complex magnetic interactions give rise to many possible magnetic states close in energy. In fact, for a dimer, we failed to locate the ground-state spin moment as spin states with moments 0, 2, and 4 μ_B are essentially degenerate.

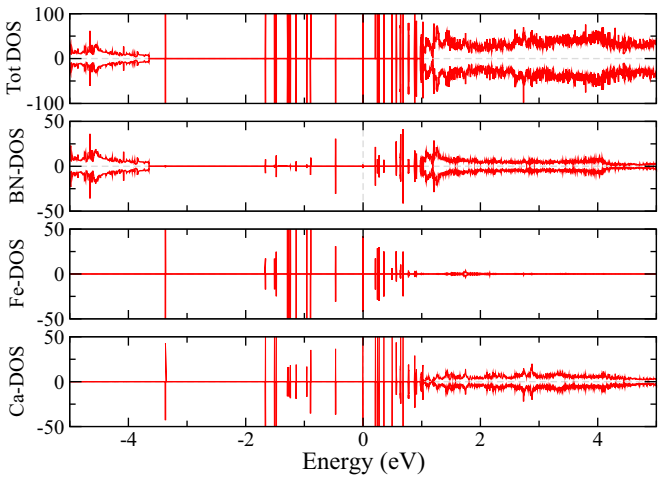

FIG. 9. (Color online) DOS of $FeCa_8$ deposited over BN-sheet using LSDA.

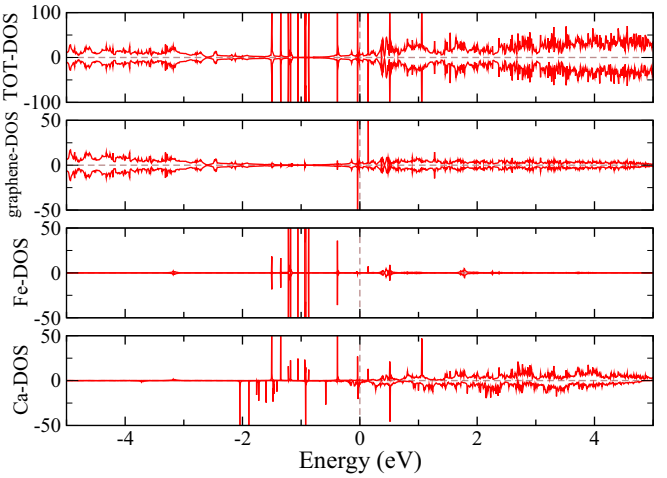

FIG. 10. (Color online) DOS of $FeCa_8$ deposited over graphene using LSDA.

IV. CONCLUSIONS

We have addressed the important question of finding the right support for assemblies of magnetic superatoms, which can be of immense importance in spintronics and other applications. It turns out that oxide substrates, which are routinely used for supporting metal clusters for catalytic reactions, are not ideal for this purpose. A calcium substrate also turns out to be interacting strongly with a $FeCa_8$ superatom so that the structure and magnetic moment of the superatom is destroyed. On the other hand, h-BN and graphene, because of their weak interactions with metal atoms and clusters, preserve the structure of the superatom in the low-energy structures. In these structures, magnetic moment of the isolated superatom is also preserved. Moreover, in a particular structure, a dimer of $FeCa_8$ superatoms on h-BN has the same moment as in the gas phase. This suggests that assemblies of $FeCa_8$ superatoms on

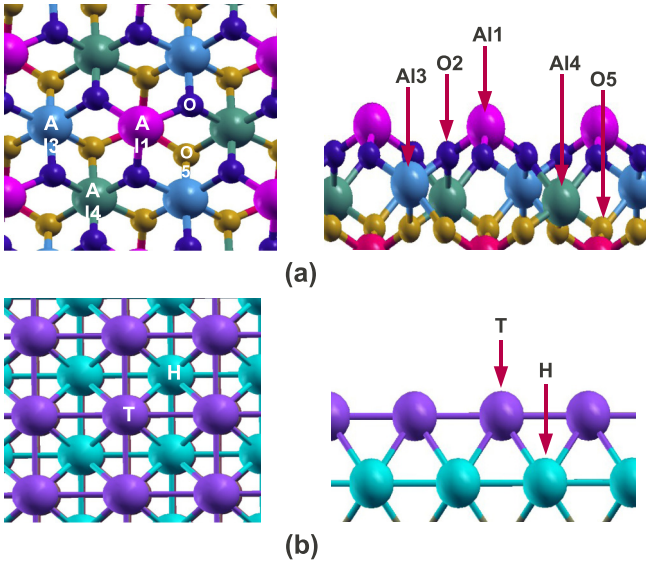

FIG. 11. (Color online) Adsorption sites of alumina and calcium surface. (Top) Alumina surface (top and side views). (Lower) Calcium surface (top and side views). Different layers are represented with different colors.

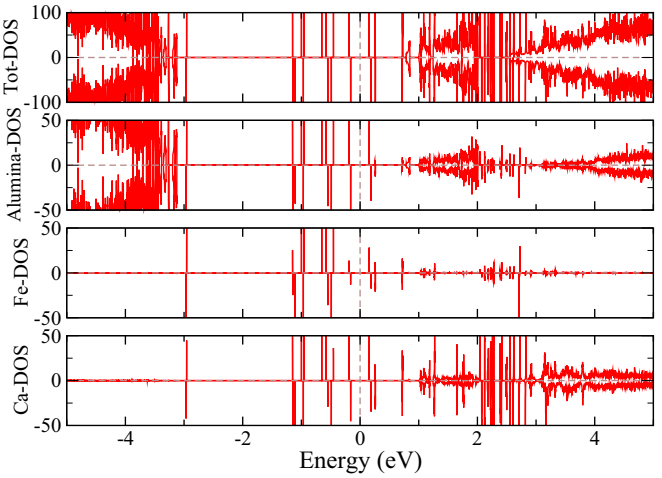

FIG. 12. (Color online) Density of states of $FeCa_8$ deposited over alumina surface.

h-BN will posses finite magnetic moments necessary for applications. We also estimated that $FeCa_8$ superatoms will remain isolated on h-BN below a coverage of 4.97×10^{13} per cm^2. Between 4.97×10^{13} and 12.73×10^{13} per cm^2 they will start forming self assemblies. This information will be useful for experimentalists. Magnetic moment of $FeCa_8$ superatoms on graphene is complicated by long range, oscillatory RKKY interactions in addition to direct exchange. The exact magnetic structure realized in a particular assembly will depend on the exact positions of all the superatoms on the substrate. In our limited explorations, we found that states with very different magnetic moments are close in energy. This may lead to magnetic frustrations and complex magnetic orders, which can be a separate topic of study. We believe that these results will motivate the experimentalists to undertake efforts to form assemblies of magnetic superatoms.

ACKNOWLEDGMENT

All the computations were done at the cluster computing facility at HRI, Allahabad (http://www.hri.res.in/cluster/).

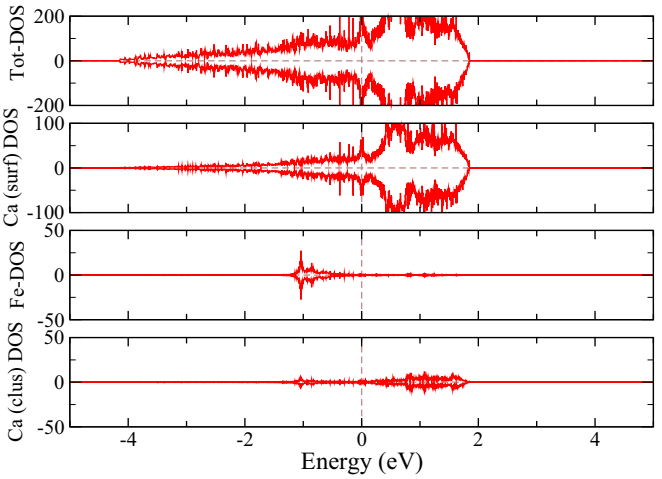

FIG. 13. (Color online) Density of states of $FeCa_8$ deposited over calcium surface.

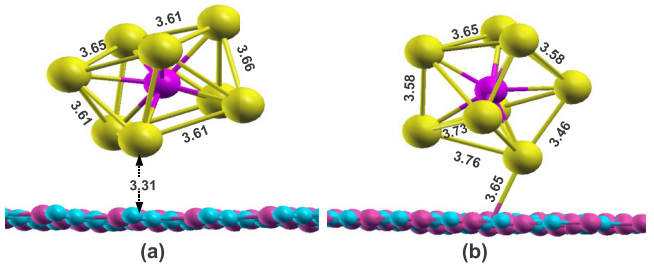

FIG. 14. (Color online) Some high-energy isomers of $FeCa_8$ deposited over BN-sheet using vdW-DF2.

APPENDIX: LSDA RESULTS

It is well known that the local density approximation (LDA, LSDA) tends to overbind systems, while the generalized gradient approximation (GGA) usually tends to underestimate binding. This is particularly acute in systems where van der Waals interactions play a major role. In the case of graphene-metal interface, GGA's predict no binding at all [33–35], which is contrary to experiments [69]. Therefore most theoretical work on graphene-metal interfaces or surface and molecular adsorption relies on the L(S)DA. The adsorption and magnetic moment of $FeCa_8$-graphene or h-BN system is modified when studied using the local density approximation.

Let us first discuss $FeCa_8$ adsorption over h-BN. We have optimized various orientations of $FeCa_8$ over different adsorption sites of a h-BN sheet using LSDA. The lowest-energy structure is obtained for an orientation where three Ca atoms are close to the substrate, shown in Fig. 8(a). In this structure, h-BN is significantly damaged by superatom deposition. One of its B atoms, which is directly below the cluster, is pulled up by 0.68 Å from the hexagonal plane. The three nearest N atoms (below the cluster) are displaced by an average of 0.29 Å from their initial positions. The maximum ΔZ_s for this case is 0.723 Å. The cluster is slightly deformed from its antiprism structure, but the overall endohedral structure is preserved. Unlike oxide and metal surfaces, Fe atom is not exposed to the surface. The minimum distance between Ca and BN-sheet atoms is found to be 2.58 Å, which is much smaller than the corresponding vdW-DF2 case. This structure has an adsorption energy $E_a = 1.49$ eV. All these facts clearly indicate that

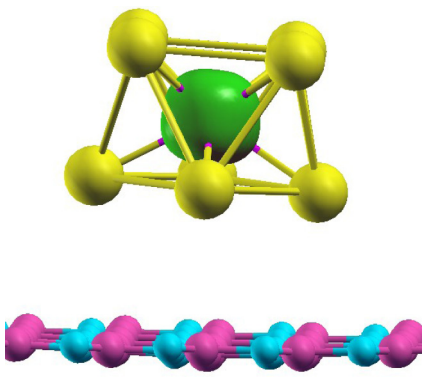

FIG. 15. (Color online) Spin density isosurface of $FeCa_8$ deposited over h-BN using vdW-DF2 (plotted at isovalue 115 a.u.).

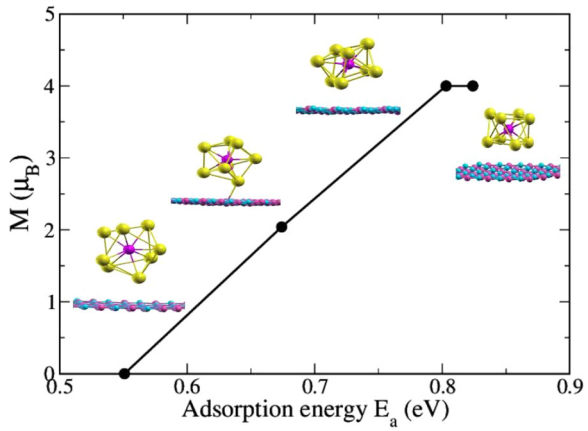

FIG. 16. (Color online) Scatter plot of adsorption energy and magnetic moment for various structures of $FeCa_8$ on h-BN. The two structures with moment 4 μ_B are the lowest-energy one and the one shown in Fig. 14(a). The one with a moment of 2 μ_B is the one in Fig. 14(b). The structure having no magnetic moment is a still higher energy one with large distortion of the antiprism cage.

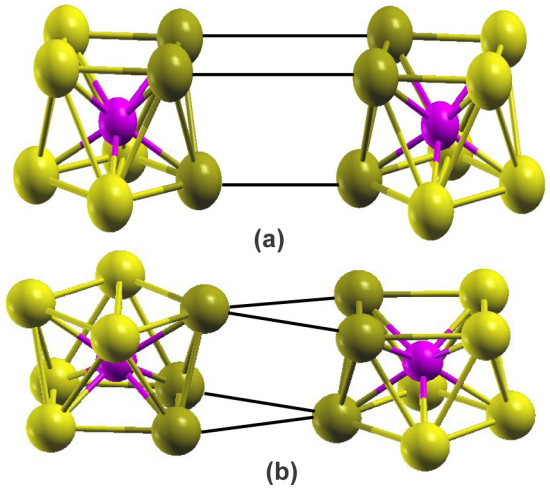

FIG. 17. (Color online) Considering the two $FeCa_8$ units are in the ground state over substrate and diffusing towards each other, we can guess two possible structures of a dimer, (a) each atom of triangular face is connected to only one atom of the other triangular face, and (b) one atom of each triangular face is connected to two atoms of the other triangular face.

LSDA predicts a strong interaction between $FeCa_8$ cluster and h-BN than the vdW-DF2 method.

In Fig. 9, similar to the vdW-DF2 case, the discrete cluster states lie within the band gap of h-BN. As interaction between cluster and h-BN is quite strong, a set of discrete states appear, which are localized on the cluster atom and the nearby substrate atoms. However, these states appear in equal numbers in both the spin channels and leave the system with no magnetic moment. Also this large interaction gives rise to a local deformation of the h-BN substrate.

Similar behavior is found for the adsorption of $FeCa_8$ over graphene when studied with LSDA. In the lowest-energy structure [Fig. 8(b)], four Ca atoms are close to the hollow and bridge sites of graphene. This structure has an adsorption energy $E_a = 3.43$ eV. The maximum relaxation Z_r and maximum ΔZ_s are found to be 0.18 and 0.22 Å, respectively. Again, we find few discrete states appearing due to cluster-substrate interaction [Fig. 10]. LSDA gives a large cluster-substrate binding, which modifies the electronic states of the cluster and leads to the loss of its moment.

[1] W. Ekardt, Phys. Rev. B **29**, 1558 (1984).
[2] W. D. Knight, K. Clemenger, W. A. de Heer, W. A. Saunders, M. Y. Chou, and M. L. Cohen, Phys. Rev. Lett. **52**, 2141 (1984).
[3] S. N. Khanna and P. Jena, Phys. Rev. B **51**, 13705 (1995).
[4] D. E. Bergeron, A. W. Castleman Jr., T. Morisato, and S. N. Khanna, Science **304**, 84 (2004).
[5] D. E. Bergeron, P. J. Roach, A. W. Castleman Jr., N. O. Jones, and S. N. Khanna, Science **307**, 231 (2005).
[6] J. U. Reveles, S. N. Khanna, P. J. Roach, and A. W. Castleman Jr., Proc. Natl. Acad. Sci. USA **103**, 18405 (2006).
[7] P. D. Jadzinsky, G. Calero, C. J. Ackerson, D. A. Bushnell, and R. D. Kornberg, Science **318**, 430 (2007).
[8] M. Walter, J. Akola, O. Lopez-Acevedo, P. D. Jadzinsky, G. Calero, Christopher J. Ackerson, R. L. Whetten, H. Grönbeck, and Hannu Häkkinen, Proc. Natl. Acad. Sci. USA **105**, 9157 (2008).
[9] V. M. Medel, J. U. Reveles, S. N. Khanna, V. Chauhan, P. Sen, and A. W. Castleman, Proc. Natl. Acad. Sci. USA **108**, 10062 (2011).
[10] X. Zhang, Y. Wang, H. Wang, A. Lim, G. Gantefoer, K. H. Bowen, J. U. Reveles, and S. N. Khanna, J. Am. Chem. Soc. **135**, 4856 (2013).
[11] J. U. Reveles, P. A. Clayborne, A. C. Reber, S. N. Khanna, K. Pradhan, P. Sen, and M. R. Pederson, Nat. Chem. **1**, 310 (2009).
[12] K. Pradhan, J. U. Reveles, P. Sen, and S. N. Khanna, J. Chem. Phys. **132**, 124302 (2010).
[13] V. Chauhan, V. M. Medel, J. U. Reveles, S. N. Khanna, and P. Sen, Chem. Phys. Lett. **528**, 39 (2012).
[14] V. Chauhan and P. Sen, Chem. Phys. **417**, 37 (2013).
[15] W. D. Knight, W. A. De Heer, W. A. Saunders, K. Clemenger, M. Y. Chou, and M. L. Cohen, Chem. Phys. Lett. **134**, 1 (1987).
[16] A. W. Castleman Jr., and S. N. Khanna, J. Phys. Chem. C **113**, 2664 (2009).
[17] F. Liu, M. Mostoller, T. Kaplan, S. N. Khanna, and P. Jena, Chem. Phys. Lett. **248**, 213 (1996).
[18] W.-J. Zheng, O. C. Thomas, T. P. Lippa, S.-J. Xu, and K. H. Bowen Jr., J. Chem. Phys. **124**, 144304 (2006).

[19] P. Clayborne, N. O. Jones, A. C. Reber, J. U. Reveles, M. C. Qian, and S. N. Khanna, J. Comp. Meth. Sci. Eng. **7**, 417 (2007).

[20] P. Melinon, V. Paillard, V. Dupuis, A. Perez, P. Jensen, A. Hoareau, M. Broyer, J. L. Vialle, M. Pellarin, B. Baguenard, and J. Lerme, Int. J. Mod. Phys. B **09**, 339 (1995).

[21] M. Pellarin, B. Baguenard, J. L. Vialle, J. Lerme, M. Broyer, J. Miller, and A. Perez, Chem. Phys. Lett. **217**, 349 (1994).

[22] P. Jensen, P. Melinon, M. Treilleux, A. Hoareau, J. X. Hu, G. Fuchs, and B. Cabaud, Nucl. Instrum. Methods Phys. Res., Sect. B **79**, 219 (1993).

[23] V. Paillard, P. Melinon, V. Dupuis, J. P. Perez, A. Perez, and B. Champagnon, Phys. Rev. Lett. **71**, 4170 (1993).

[24] P. Kéghélian, P. Mélinon, A. Perez, J. Lermé, C. Ray, M. Pellarin, M. Broyer, J. L. Rousset, F. J. Cadete, and Santos Aires, Eur. Phys. J. D **9**, 639 (1999).

[25] J. P. Perez, V. Dupuis, J. Tuaillon, A. Perez, V. Paillard, P. Melinon, M. Treilleux, L. Thomas, B. Barbara, and B. Bouchet-Fabre, J. Magn. Magn. Mater. **145**, 74 (1995).

[26] F. Parent, J. Tuaillon, L. B. Stern, V. Dupuis, B. Prevel, A. Perez, P. Melinon, G. Guiraud, R. Morel, A. Barthélémy, and A. Fert, Phys. Rev. B **55**, 3683 (1997).

[27] J. Tuaillon, V. Dupuis, P. Mélinon, B. Prével, M. Treilleux, A. Perez, M. Pellarin, J. L. Vialle, and M. Broyer, Philos. Mag. A **76**, 493 (1997).

[28] G. Fuchs, P. Melinon, M. Treilleux, and J. Le Brusq, J. Phys. D Appl. Phys. **26**, 143 (1993).

[29] H. He, R. Pandey, J. U. Reveles, S. N. Khanna, and S. P. Karna, Appl. Phys. Lett. **95**, 192104 (2009).

[30] J. L. Chen, C. S. Wang, K. A. Jackson, and M. R. Pederson, Phys. Rev. B **44**, 6558 (1991).

[31] I. M. L. Billas, A. Châtelain, and W. A. de Heer, Science **265**, 1682 (1994).

[32] C. R. Dean, A. F. Young, I. Meric, C. Lee, L. Wang, S. Sorgenfrei, K. Watanabe, T. Taniguchi, P. Kim, K. L. Shepard, and J. Hone, Nat. Nanotechnol. **5**, 722 (2010); S. Tang, H. Wang, Y. Zhang, A. Li, H. Xie, X. Liu, L. Liu, T. Li, F. Huang, X. Xie, and M. Jiang, Sci. Rep. **3**, 2666 (2013).

[33] M. Amft, S. Lebègue, O. Eriksson, and N. V. Skorodumova, J. Phys.: Condens. Matter **23**, 395001 (2011).

[34] J.-P. Jalkanen, M. Halonen, D. Fernández-Torre, K. Laasonen, and L. Halonen, J. Phys. Chem. A **111**, 12317 (2007).

[35] M. Vanin, J. J. Mortensen, A. K. Klkkanen, J. M. Garcia-Lastra, K. S. Thygesen, and K. W. Jacobsen, Phys. Rev. B **81**, 081408 (2010).

[36] M. Bokdam, G. Brocks, M. I. Katsnelson, and P. J. Kelly, Phys. Rev. B **90**, 085415 (2014).

[37] J. G. Díaz, Y. Ding, R. Koitz, A. P. Seitsonen, M. Iannuzzi, and J. Hutter, Theor. Chem. Acc. **132**, 1350 (2013).

[38] P. Gehring, B. F. Gao, M. Burghard, and K. Kern, Nano Lett. **12**, 5137 (2012).

[39] P. E. Blöchl, Phys. Rev. B **50**, 17953 (1994).

[40] G. Kresse and D. Joubert, Phys. Rev. B **59**, 1758 (1999).

[41] J. Neugebauer and M. Scheffler, Phys. Rev. B **46**, 16067 (1992).

[42] G. Kresse and J. Hafner, Phys. Rev. B **47**, 558 (1993); **49**, 14251 (1994); G. Kresse and J. Furthmuller, J. Comput. Mat. Sci. **6**, 15 (1996); Phys. Rev. B **54**, 11169 (1996); G. Kresse, Ph.D. thesis, Technische Universit at Wien, 1993.

[43] S. Grimme, J. Comput. Chem. **25**, 1463 (2004).

[44] S. Grimme, J. Comput. Chem. **27**, 1787 (2006).

[45] S. Grimme, J. Antony, S. Ehrlich, and H. Krieg, J. Chem. Phys. **132**, 154104 (2010).

[46] D. C. Langreth, B. I. Lundqvist, S. D. Chakarova-Käck, V. R. Cooper, M. Dion, P. Hyldgaard, A. Kelkkanen, J. Kleis, L. Kong, S. Li *et al.*, J. Phys.: Condens. Matter **21**, 084203 (2009).

[47] H. Rydberg, B. I. Lundqvist, D. C. Langreth, and M. Dion, Phys. Rev. B **62**, 6997 (2000).

[48] H. Rydberg, M. Dion, N. Jacobson, E. Schröder, P. Hyldgaard, S. I. Simak, D. C. Langreth, and B. I. Lundqvist, Phys. Rev. Lett. **91**, 126402 (2003).

[49] M. Dion, H. Rydberg, E. Schröder, D. C. Langreth, and B. I. Lundqvist, Phys. Rev. Lett. **92**, 246401 (2004).

[50] M. Dion, H. Rydberg, E. Schröder, D. C. Langreth, and B. I. Lundqvist, Phys. Rev. Lett. **95**, 109902 (2005).

[51] A. Singh, C. Majumder, and P. Sen, J. Chem. Phys. **140**, 164705 (2014).

[52] K. Lee, E. D. Murray, L. Kong, B. I. Lundqvist, and D. C. Langreth, Phys. Rev. B **82**, 081101 (2010).

[53] J. Klimes, D. R. Bowler, and A. Michaelides, J. Phys.: Condens. Matter **22**, 022201 (2010).

[54] J. Klimes, D. R. Bowler, and A. Michaelides, Phys. Rev. B **83**, 195131 (2011).

[55] Y. Zhang and W. Yang, Phys. Rev. Lett. **80**, 890 (1998).

[56] N. Godbout, D. R. Salahub, J. Andzelm, and E. Wimmer, Can. J. Chem. **70**, 560 (1992).

[57] J. P. Perdew, K. Burke, and M. Ernzerhof, Phys. Rev. Lett. **77**, 3865 (1996).

[58] P. Thomson, D. E. Cox, and J. B. Hastings, J. Appl. Crystallogr. **20**, 79 (1987).

[59] R. H. French, J. Am. Ceram. Soc. **73**, 477 (1990).

[60] G. Henkelman, A. Arnaldsson, and H. Jónsson, Comput. Mater. Sci. **36**, 354 (2006).

[61] W. B. Pearson, A Handbook of Lattice Spacing and Structures of Metals and Alloys **2**, 81 (1958).

[62] K. Watanabe, T. Taniguchi, and H. Kanda, Nat. Mater. **3**, 404 (2004).

[63] S. Saremi, Phys. Rev. B **76**, 184430 (2007).

[64] A. M. Black-Schaffer, Phys. Rev. B **81**, 205416 (2010).

[65] S. R. Power and M. S. Ferreira, Crystals **3**, 49 (2013).

[66] H. Chen, Q. Niu, Z. Zhang, and A. H. MacDonald, Phys. Rev. B **87**, 144410 (2013).

[67] P. O. Lehtinen, A. S. Foster, A. Ayuela, A. Krasheninnikov, K. Nordlund, and R. M. Nieminen, Phys. Rev. Lett. **91**, 017202 (2003).

[68] A. Nag, K. Raidongia, K. P. S. S. Hembram, R. Datta, U. V. Waghmare, and C. N. R. Rao, ACS Nano **4**, 1539 (2010).

[69] R. Rosei, M. De Crescenzi, F. Sette, C. Quaresima, A. Savoia, and P. Perfetti, Phys. Rev. B **28**, 1161(R) (1983).